

New Tool for Detection and Prediction of Major Depressive Disorder

Pallabjyoti Kakoti, Rissnalin Syiemlieh, and Eeshankur Saikia

Department of Applied Sciences, Gauhati University, Guwahati 781014, India

ABSTRACT

KEYWORDS

multifractal analysis
cognition
depression
major depressive disorder,
fMRI
nonlinear dynamics

Though there has been immense progress in the field, early detection and reliable prediction of major depressive disorder (MDD) still remains a challenge. In the present study, we used multi fractal analysis (MFA) to perform statistical analysis on fMRI resting-state data of depressed patients and normal controls to find out the singularity spectrum, an important tool of MFA, and derive various supporting attributes, leading to a quantification of the geometrical pattern formation in the brain. It was found, and reported for the first time, that the estimates of Hurst exponent and fractal dimension values vary significantly for the depressed subjects and normal controls, helping in detecting and predicting early signs of depression.

INTRODUCTION

The key characteristic of major depressive disorder (MDD) is chronic and prevalent low mood. Several other variables determine the entire syndrome. They may be categorized into behavioral, emotional, neurological, and biological characteristics. Extreme cases are related to psychotic characteristics (Cleare et al., 2012). Researchers have found that depression is accompanied by a large cognitive functional defect, which has been shown in issues with mental functioning such as planning ability, problem solving, working memory, and processing speed (Chakrabarty et al., 2016; Mitchell, 2016). However, other researches showed no significant variations between participants with or without depression (Grant et al., 2001). One study (Alloy & Abramson, 1979) concluded that depressed patients at times are "sadder yet smarter" than persons without a psychopathological background. The authors noticed

that nondepressed people displayed cognitive bias that promoted constructive interpretations of the self and the environment, while depressed people held a rational, though pessimistic, perception that probably contributed to their negative mood (Alloy & Abramson, 1979). The use of resting-state functional magnetic resonance imaging (fMRI) to explain the pathophysiological processes causing affective and cognitive dysfunctions in MDD is gaining prominence (Veer, 2010; Zeng et al., 2012). At rest, the default mode network and the affective network in depressive patients were shown to be abnormal (Sheline et al., 2010; Zeng et al.,

Corresponding author: Eeshankur Saikia, Department of Applied Sciences, Gauhati University, Guwahati 781014, India.
Email: eeshankur@gauhati.ac.in

2012; Zhou et al., 2010). In one study, depressed patients had a smaller left medial frontal pole, which was found to have a negative correlation with disease duration and severity. (Bludau et al., 2015). This suggests that MDD serves many biologically distinct disorders and a single marker could serve a function that encompasses all biological pathways to detect depression which could be extracted from brain signals. The signals captured by fMRI are highly dynamic and nonlinear. While research has been conducted to access internal states through behavioral studies by the use of AI in autism (Bartlett et al., 2019), in case of MDD, such studies have shown encouraging preliminary results only and need further validation (Swan et al., 2014).

The current study applied multi fractal analysis (MFA) for differentiating between the fractality of MDD subjects and healthy controls. The MFA is the investigation of how a vector spreads through a geometric support, like a volume or fractal. In fact, multifractals are "infinite sets of exponents" that reflect the scale (power law) of all the moments of distribution of the quantities described by the fractal structure. The exponent is taken from a power law and used to describe and forecast an unexpected event during the analysis. This has been used to examine a variety of real-life situations, including foreign exchange data, cancer detection by probing multifractality in the tissue refractive index, and brain functional connectivity (Das et al., 2013, 2014; Schmitt et al., 1999; Varley et al., 2020).

Early research showed that spontaneous neuronal activity has scale-free characteristics, implying the resting-state blood-oxygen-level-dependent (BOLD) signal's temporal complexity and fractality (Ciuciu et al., 2012; Friston et al., 2004). By describing the self-similarity of time courses, fractal dimension reflects scale-free characteristics. The Hurst exponent (H) is a metric of temporal dynamics "long-term memory" that is usually correlated to the fractal dimension and measures the consistent or anti-persistent (past patterns appear to revert in the future) behavior of a time series. It decides whether the given time series is absolutely random or has any long-term memory. The predominance of long-term memory in cortical areas, indicating more usual dynamics, was indicated for early Alzheimer's disease (Maxim, 2005), whereas a change to lower H was showed to indicate autism (Lai et al., 2010). The above results clearly demonstrate the significance of understanding natural and abnormal neuronal mechanisms with scale-free properties of intrinsic neural activity which can be investigated using Hurst exponents.

Here, we used resting-state fMRI data from patients with MDD and healthy controls, which exposed inherent, random networks that illustrate the brain's functional architecture, to compare their BOLD signals. We preprocessed the data for estimation and elimination of noise components to prevent spurious associations based on non-neuronal sources, and we performed a further connectivity analysis for regions of interests (ROI) to estimate the correlations for each pair of source and ROI by temporal-filtering and windowing the BOLD data which, in turn, provided a hemodynamical contrast signal for the voxel of interest (VOI) for both MDD and control patients. Through an examination of the fractality and persistency of the BOLD time series, we hypothesized that the ruminative nature of depression would be represented in the hemodynamical response of the left frontal pole.

MATERIALS AND METHODS

The fMRI data of 30 subjects were taken out of 72 subjects with age ranging from 19 to 50 years, of both genders, and having demographic similarity, from a study by Bezmaternykh et al. (2020). Out of 30 subjects, 15 were diagnosed with MDD and the rest of them were assigned as controls with no history of MDD. Resting-state fMRI data with closed eyes along with structural MRI data were collected at a session consisting of 100 dynamic scans with the repetition time of 2.5 s and 25 slices with structural images at 1 mm isotropic resolution in the sagittal plane. Resting-state studies of sporadic fluctuations in the fMRI BOLD signals have shown advances in mapping the broad inherent functional architecture of the brain. Regions with identical functional connectivity, even in the absence of external sensory input or motor response, display temporally coherent BOLD fluctuations (Beckmann et al., 2005; Biswal et al., 1995; Cordes et al., 2000). Negative associations between brain regions with theoretically opposing functional roles have also been studied (Fox, 2005; Fransson, 2005; Kelly et al., 2008).

fMRI Preprocessing and Functional Analysis

The resulting fMRI images were preprocessed using the CONN functional connectivity toolbox (Whitfield & Nieto, 2012), which uses statistical parametric mapping (Friston et al., 2007) and MATLAB (v9.3.0, 2017). Head motion artifacts, in addition to physiological distortions, have been demonstrated to have a considerable impact on intrinsic functional connectivity measures (Satterthwaite et al., 2012; Van Dijk et al., 2012). The subjects' mean and maximum motion of the head inside the scanner were computed (see Table 1). The fact that depressed subjects had more motion than controls suggests that motion-related changes in brain connectivity are not entirely due to motion artefacts, but rather represent individual differences in functionality (Van Dijk et al., 2012; Zeng et al., 2014).

The functional data was realigned and unwrapped, with all scans coregistered and rescaled to a reference image utilizing b-spline interpolation (Anderson et al. 2001), which addresses potential distortion-by-motion interactions by calculating the derivatives of the displacement with respect to head motion and rescaling the functional data to fit the reference image's displacement field (see Figure 1). Using sinc interpolation resampling and time-shifting, slice-timing correction (Henson et al. 1999) was utilized to correct the temporal misalignment between the different slices of functional data. After that, from the observed global BOLD signal, potential outlier scans were detected and framewise displacement was estimated at each timepoint, with the signal scaled to SD units. The functional and structural data were then separated into grey matter, white matter, and cerebrospinal fluid tissue classes after being normalized into standard Montreal Neurological Institute (MNI) space (see Figure 2; see also Ashburner & Friston, 2005).

Component-based noise correction was used to introduce denoising. The CompCor (Behzadi et al., 2007) technique was used to extract the signal's first five principal components from the white matter and cerebrospinal fluid masks, as well as six motion parameters and their

TABLE 1.

Subjects' Demographic Data along with Mean and Maximum Head Motion inside the MRI Scanner Disregarding Outlier Scans

Subject	Category	Age/Gender	Mean Head Motion	Max Head Motion
1	MDD	50 / M	0.06	0.12
2	MDD	32 / F	0.08	0.31
3	MDD	26 / F	0.07	0.18
4	MDD	28 / F	0.08	0.17
5	MDD	28 / M	0.07	0.33
6	MDD	52 / F	0.13	1.27
7	MDD	24 / M	0.19	0.19
8	MDD	28 / M	0.09	0.16
9	MDD	29 / F	0.15	1.39
10	MDD	34 / F	0.09	0.52
11	MDD	44 / F	0.05	0.12
12	MDD	31 / F	0.09	0.33
13	MDD	28 / M	0.06	0.18
14	MDD	45 / F	0.09	0.24
15	MDD	47 / F	0.10	1.13
16	Control	32 / M	0.04	0.15
17	Control	44 / F	0.11	0.49
18	Control	26 / F	0.15	0.31
19	Control	31 / F	0.06	0.38
20	Control	31 / M	0.07	0.27
21	Control	47 / F	0.04	0.12
22	Control	31 / M	0.04	0.32
23	Control	24 / F	0.09	0.43
24	Control	34 / F	0.07	0.21
25	Control	30 / F	0.11	0.49
26	Control	39 / M	0.12	0.79
27	Control	37 / F	0.11	0.41
28	Control	43 / F	0.06	0.15
29	Control	34 / F	0.09	0.58
30	Control	52 / F	0.09	0.23

first order temporal derivatives, a linear detrending term, and smoothing. As compared to approaches that focus on global signal regression, the CompCor noise reduction approach allows for the identification of anticorrelations because no global data is regressed, increasing the fMRI analysis' sensitivity and selectivity. Denoising was achieved with a band-pass filter size of [0.008, 0.09] Hz and a 6 mm smoothing kernel. Additionally, movement and temporal covariates were removed, and the residual BOLD time series was temporal filtered and windowed.

First level functional connectivity analyses were performed for all ROIs and seed-to-voxel analyses to generate a hemodynamical response function weighted generalized linear modelling (GLM) using bivariate correlation, which has been computed separately for each pair of source and target ROIs.

Estimation of Singularity Spectrum

A continuum of exponents is needed to define a dynamical monofractal or multifractal system, known as a singularity spectrum. The range of points is measured by a specified regularity exponent α , known as the Hölder exponent (McCauley, 1993), when the output spectrum $f(\alpha)$ is generated, which is defined by

$$\alpha = \log \mu(\text{box}) / \log \varepsilon \quad (1)$$

where $\mu(\text{box})$ is the measure of the box, and ε is the dimension of the box. α values are similar to the respective fractal dimension of the dynamical system observed. The local Hölder exponent at a certain time quantifies the local scaling properties of the process (local divergence). In other words, the local regularity of the process is calculated. The distribution of Hölder exponents degenerates in conventional time series models and converges to a single point, whereas multi-fractals are defined by a continuum of Hölder exponents. We can count boxes having dimension ε for every α value with its rough estimate of Hölder exponent equal to α and take the value as $N_\varepsilon(\alpha)$. Then, the Hausdorff dimension for α distribution is characterized as

$$f_\varepsilon(\alpha) = -\frac{\log N_\varepsilon(\alpha)}{\log \varepsilon} \quad (2)$$

The singularity spectrum is the curve spanning fractal dimensions such as, the one expressed in Equation 2 and Hölder's exponent α , where the breadth of the $\Delta\alpha_\varepsilon$ spectrum captures the shape of the multifractal continuum of singularities and determines the probability distribution, and the Δf_ε dimension difference quantifies the fractals' self-similarity (Saha et al., 2020). In the case of monofractals, the spectrum converges in a one-point source but becomes a bell-shaped structure with downward roots for a multifractal scheme. The value of α provides local information on pointwise continuity, while the value of $f_\varepsilon(\alpha)$ provides global information.

Thus, the greater the value of $\Delta\alpha$, the greater the likelihood of self-similarity increases at different geometrical scale. This suggests coherence of the neuronal firings in the brain, since higher fractal dimension $\Delta f(\alpha)$ is a marker of richer geometry or texture, resulting in richer patterns. In turn, this suggests uniformity at different neurological scales. Therefore self-similarity can be established in the fMRI data considered.

The current study was based on the measurement of Hölder exponent at each point of the BOLD time series to obtain the singularity spectrum for each subject. The MFA was carried out using the FracLab package in MatLab for generating the Hölder exponents for the time series and plotting the Legendre spectrum (Véhel & Legrand, 2004).

Estimation of Hurst Exponent:

We followed the rescaled range approach (R/S, Mandelbrot & Wallis, 1968) for calculating the Hurst exponent, which varies on the power law (Suyal et al., 2009).

$$(R/S)_w = kw^H \quad (3)$$

Where k is the constant, w is the width of the time window, and S is the standard deviation of the independent variable x_i within the window w , which is given by

$$|S(t_0, w)|^2 = \frac{1}{w-1} \sum_{i=t_0}^{t_0+w-1} [x_i - \bar{x}(t_0, w)]^2 \quad (4)$$

with the average value of the independent variable x_i as,

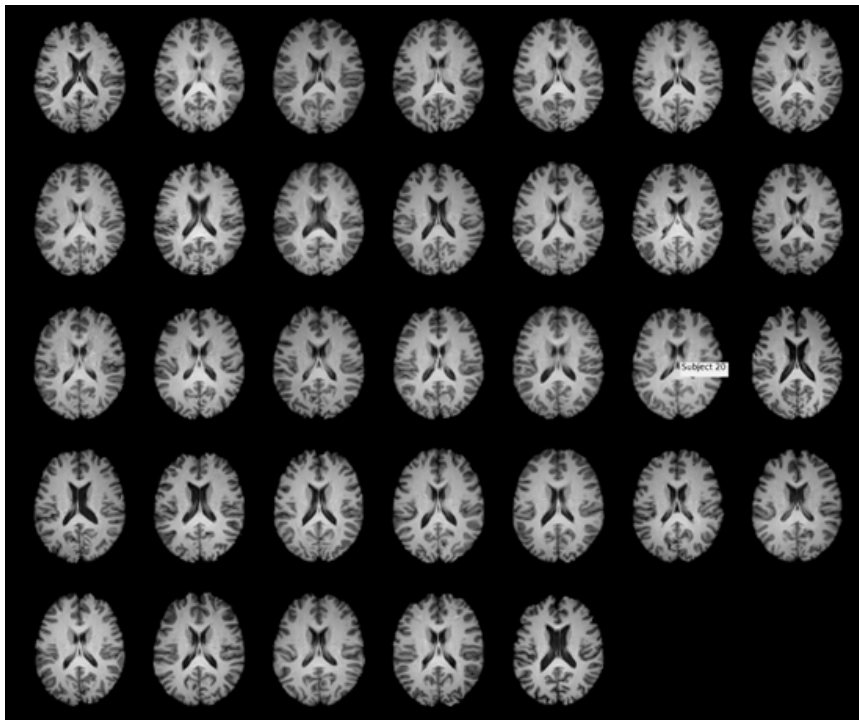
$$\bar{x}(t_0, w) = \frac{1}{w} \sum_{i=t_0}^{t_0+w-1} x_i \quad (5)$$

and R , the range in the time-series, defined as

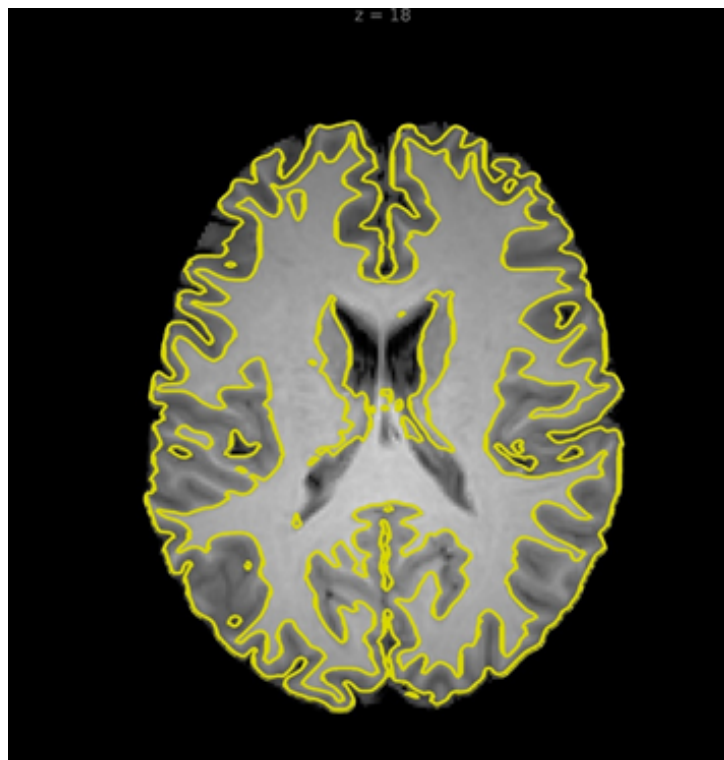
$$R(t_0, w) = \max_1 \leq i \leq w y_i(t_0, w) - \min_1 \leq i \leq w y_i(t_0, w) \quad (6)$$

With the new variables $y_i, i = 1, 2, 3, \dots, w$ as

$$y_i(t_0, w) = \sum_{k=t_0}^{t_0+i-1} [x_k - \bar{x}(t_0, w)] \quad (7)$$

**FIGURE 1.**

Single slice montage of structural MRI of the subjects in x-y plane after the realignment of scans co-registered and rescaled to a reference image utilizing b-spline interpolation.

**FIGURE 2.**

Single slice of structural MRI of Subject 13 with overlay of grey matter, white matter, and cerebrospinal fluid tissue class segmentation after being normalized into standard Montreal Neurological Institute space.

For different time instances, (R/S) is calculated and averaged in for epochs and plotted against w on a log-log axis (Constantine & Percival, 2017). The slope of the linear regression gives the value of H which lies between the values of 0 and 1. A value of $H = 0.5$ represents a pure random walk/Brownian motion of the time series. An H between 0.5 and 1.0 denotes a consistent time series. A greater H than that means that the time series has a higher long-term positive autocorrelation and a longer memory, that is, more frequent or consistent deviations. Antipersistence is indicated by an H between 0 and 0.5, and random time series is indicated by an H more or less equal to 0.5 (Suyal et al., 2009).

Estimation of Fractal Dimension

A fractal dimension is a metric for quantifying the complexity of fractal patterns or sets by comparing the change in complexity to the change in size. It is described as a rough or fragmented geometric form that can be subdivided into smaller sections (Li et al., 2002; Falconer, 2007). Fractal systems (such as time series) do not have a single time scale, just as fractal structures do not have a single length scale (Li et al., 2002). Fractal theory provides tools for explaining natural objects' intrinsic irregularity. The fractal dimension, denoted by D , is a constant parameter that characterizes this theory (Li et al., 2002). The common definition of fractal dimension, D being a special case, based on the covering method (Farshad & Ahmadi, 1974; Kaplan & Glass, 1996) as $\epsilon > 0$, an ϵ -cover of X is a finite collection of spherical balls $B_i \subset \mathbb{R}^d$ of a diameter $|B_i| \leq \epsilon$ that covers X

$$H^\delta(X) = \lim_{\delta \rightarrow 0} f \left[\sum_{i=1}^{\infty} |B_i|^\delta \right] \quad (8)$$

Where $i = 1, 2, 3, \dots, H^\delta(X)$ denotes the δ -dimensional Hausdorff (Falconer, 2007; Grassberger & Procaccia, 1983) measure of X , there exists a nonnegative value D such that $H^\delta(X) = \infty$ if $\delta < D$ and $H^\delta(X) = 0$ if $\delta > D$. The Hausdorff dimension coincides with the box-count dimension under weak regularity conditions (Kaplan & Glass, 1996), that is,

$$D = \lim_{\epsilon \rightarrow 0} \frac{\log N(\epsilon)}{\log(\frac{1}{\epsilon})} \quad (9)$$

Where $N(\epsilon)$ denotes the smallest number of cubes of width ϵ in \mathbb{R}^d which can cover X . The basic concept is straightforward: a single box covers the time series graph initially. After the box is split into four quadrants, the number of cells needed to cover the curve is calculated. The next quadrant is divided into four sub-quadrants, and so on until the box width equals the data resolution, keeping track of the number of quadrants needed to cover the graph at each point. The box-count estimator equals the slope in an ordinary least squares regression t of $\log N(\epsilon)$ on $\log(\epsilon)$ if $N(\epsilon)$ denotes the number of boxes needed at width or scale ϵ (Farshad & Ahmadi, 1974).

RESULTS AND DISCUSSION

After generating cluster-based inferences for both MDD patients and healthy controls by implementing Gaussian random field theory parametric statistics in group-level seed-to-voxel connectivity measures (bivariate correlation), we observed major differences in functional BOLD activation in the left frontal pole cortex (see Figure 3).

Taking the left frontal pole cortex as the candidate for fractal analysis due to its high variance, multivariate BOLD time series was extracted for the largest VOI cluster having a size of 21796 voxels for healthy controls and 20092 voxels for MDD subjects. Also, high anticorrelating functional connectivity differences were seen in the inferior frontal gyrus among MDD patients and healthy controls. The inferior frontal gyrus is responsible for language processing and speech production, and this result needs to be investigated further.

The Hölder exponent α for all subjects was determined (see Figure 4). The $f(\alpha)$ was higher for healthy controls than for MDD patients (see Table 2), which shows that, in case of controls, coherency of fractality across different dimensions was higher, and it was greatly reduced in case of MDD patients.

Furthermore, for the MDD patients, the fractal dimension D was more random because of a larger degree of freedom shown by the system. For controls, however, due to the lower randomness, the fractal dimension was smaller. The Hurst Exponent H also indicated directly that the MDD time series were more random and less persistent.

The number of degrees of freedom exhibited by a physical system is widely used to determine its complexity. However, it is necessary to differentiate between theoretical value and effective degrees of freedom showing up.

Despite the fact that there might be many degrees of freedom available for the system, the mechanics of the system will coordinate the motion into just a few effective ones by self-organization. Self-organization occurs in dissipative dynamical systems with fewer degrees of freedom than are nominally available after transient action. The system is drawn to a lower-dimensional phase space, whose dimension reflects the number of active degrees of freedom in the self-organized system. A system that appears to be complex can actually stabilize into a chaotic yet low-dimensional state. The reason for quantifying chaos is to differentiate irregular but low-dimensional behavior from completely irregular behavior, which is stochastic in nature, possessing many effective degrees of freedom. The main motivation for estimating the fractal dimension for the MDD and control subjects was to see if depression leads to increased degrees of freedom of the depressed mind-state and a drop in the self-organizational properties as evident from D and $f(\alpha)$.

To sum up, the results from fractal dimension, Hurst exponent and Holder's exponent complement each other to add to our existing understanding that MDD can lead to changes in the fractality of the brain, leading to more randomness of neural firings and thus an increase in the fractal dimension when compared to healthy controls. A Hurst exponent of 0.5 also indicates Brownian motion / random walk of the time series, as a result of loss of brain persistence, when the subject loses information, requiring higher degrees of freedom and hence higher dimensional fractality.

TABLE 2.

Singularity Spectra Parameters, Fractal Dimension, Hurst Exponent Estimations

Subject State	$\Delta f(\alpha)$	$\Delta \alpha$	Fractal dimension (D)	Hurst exponent (H)
Control	0.52	0.44	1.2	0.742
MDD	0.19	0.59	1.6	0.582

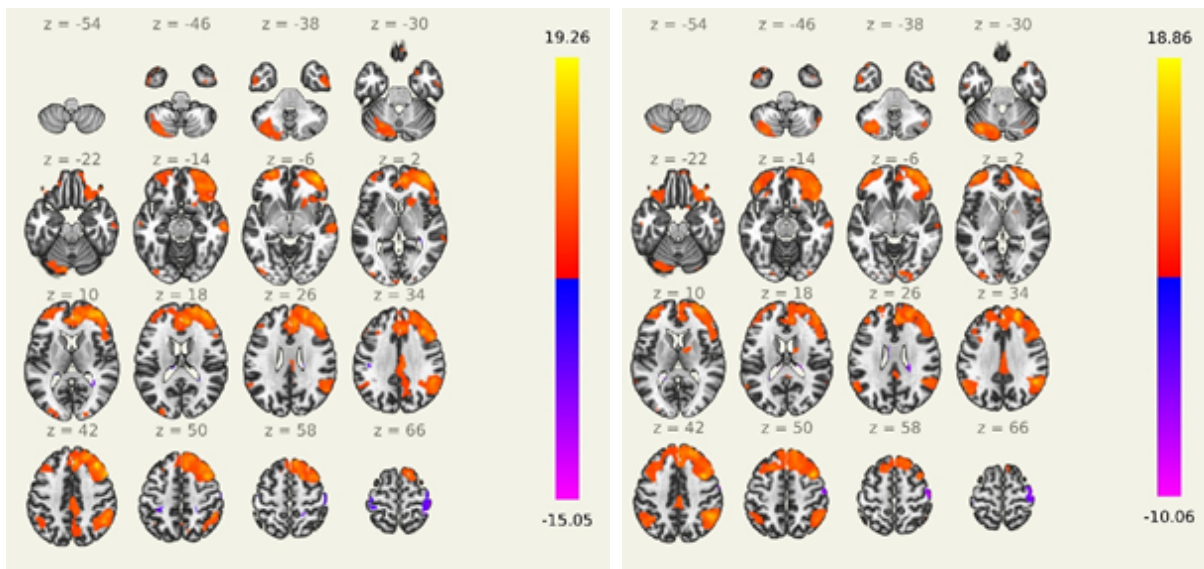


FIGURE 3.

Multi-slice display showing the left-frontal-pole functional blood oxygen level dependent activation maps of major depressive disorder subjects having voxel size 20092 and Montreal Neurological Institute coordinates (36,30,40; left panel) and control subjects having voxel size 21796 (right panel) and coordinates (20,60,-10) calculated from group-level seed-to-voxel connectivity measures (bivariate correlation).

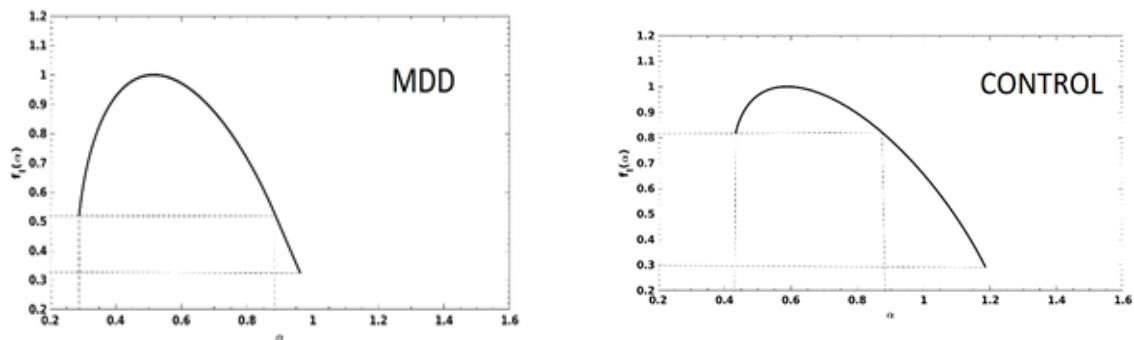


FIGURE 4.

Legendre spectrum for major depressive disorder (MDD) and control subjects plotted between values of Hausdorff dimension $f_{\epsilon}(\alpha)$ and Hölder's exponent α , for which the width of the $\Delta\alpha_{\epsilon}$ spectrum captures the form of the multi-fractal continuum of singularities and defines the distribution of probabilities

CONCLUSIONS

We used MFA to perform a statistical analysis on fMRI resting-state data from depressed patients and healthy controls, evaluating the fractal dimension, Hurst exponent and Holder's exponent, in order to quantify the geometrical pattern formation in the brain. It has been discovered that in the case of MDD, the fractality of the BOLD time series decreases. The Hurst exponent and fractal dimension estimates, on the other hand, indicate that in the case of MDD, the randomness or unpredictable aspect of the time series increases, reducing the fractal richness of the patterns. This quantification may be used for modelling, aiding rapid diagnosis of depression.

ACKNOWLEDGEMENTS

We are thankful to Bezmaternykh DD, Melnikov ME, Savelov AA & Petrovskii ED for sharing the data. PK & RS express gratitude to the Ministry of Human Resource Development (MHRD), Govt of India, for a fellowship under the World Bank funded project TEQIP-III.

REFERENCES

- Alloy, L. B., & Abramson, L. Y. (1979). Judgment of contingency in depressed and nondepressed students: Sadder but wiser? *Journal of Experimental Psychology: General*, 108, 441–485. doi: 10.1037/0096-3445.108.4.441
- Anderson, A. W., Marois, R., Colson, E. R., Peterson, B. S., Duncan, C. C., Ehrenkranz, R. A., . . . Ment, L. R. (2001). Neonatal audi-

- tory activation detected by functional magnetic resonance imaging. *Magnetic Resonance Imaging*, 19, 1–5. doi: 10.1016/s0730-725x(00)00231-9
- Ashburner, J., & Friston, K. J. (2005). Unified segmentation. *NeuroImage*, 26, 839–851. doi: 10.1016/j.neuroimage.2005.02.018
- Bartlett, M., Garcia, D. H., Thill, S., & Belpaeme, T. (2019). Recognizing human internal states: A conceptor-based approach. *arXiv:1909.04747*.
- Beckmann, C. F., DeLuca, M., Devlin, J. T., & Smith, S. M. (2005). Investigations into resting-state connectivity using independent component analysis. *Philosophical Transactions of the Royal Society B: Biological Sciences*, 360, 1001–1013. doi: 10.1098/rstb.2005.1634
- Behzadi, Y., Restom, K., Liau, J., & Liu, T. T. (2007). A component based noise correction method (CompCor) for BOLD and perfusion based fMRI. *NeuroImage*, 37, 90–101. doi: 10.1016/j.neuroimage.2007.04.042
- Bezmaternykh, D. D., Melnikov, M. E., Savelov, A. A., & Petrovskii, E. D. (2020). Resting state with closed eyes for patients with depression and healthy participants. *OpenNeuro* [Dataset]. doi: 10.18112/openneuro.ds002748.v1.0.3
- Biswal, B., Zerrin Yetkin, F., Haughton, V. M., & Hyde, J. S. (1995). Functional connectivity in the motor cortex of resting human brain using echo-planar MRI. *Magnetic Resonance in Medicine*, 34, 537–541. doi: 10.1002/mrm.1910340409
- Bludau, S., Bzdok, D., Gruber, O., Kohn, N., Riedl, V., Sorg, C., . . . Amunts, K. (2016). Medial prefrontal aberrations in major depressive disorder revealed by cytoarchitecturally informed voxel-based morphometry. *American Journal of Psychiatry*, 173, 291–298. doi: 10.1176/appi.ajp.2015.15030349
- Chakrabarty, T., Hadjipavlou, G., & Lam, R. W. (2016). Cognitive dysfunction in major depressive disorder: Assessment, impact, and management. *FOCUS*, 14, 194–206. doi: 10.1176/appi.focus.20150043
- Ciuciu, P., Varoquaux, G., Abry, P., Sadaghiani, S., & Kleinschmidt, A. (2012). Scale-free and multifractal time properties of fMRI signals during rest and task. *Frontiers in Physiology*, 3, 186. doi: 10.3389/fphys.2012.00186
- Cleare, A., Fekadu, A., & Rane, L. (2012). Unipolar depression. In P. Wright, J. Stern, & M. Phelan (Eds.), *Core psychiatry* (pp. 287–311). W. B. Saunders.
- Constantine, W., & Percival, D. (2017). *fractal: A fractal time series modeling and analysis package, version 2.0-4*.
- Cordes, D., Haughton, V., Arfanakis, K., Wendt, G., Turski, P. A., Moritz, C., . . . & Meyerand, M. (2000). Mapping functionally related regions of brain with functional connectivity MRI (fcMRI). *American Journal of Neuroradiology*, 21, 1636–44.
- Kaplan, D., & Glass, L. (1996). *Understanding nonlinear dynamics*. Springer.
- Das, N., Chatterjee, S., Soni, J., Jagtap, J., Pradhan, A., Sengupta, T. K., . . . & Ghosh, N. (2013). Probing multifractality in tissue refractive index: Prospects for precancer detection. *Optics Letters*, 38, 211–213.
- Das, N., Chatterjee, S., Chakraborty, S., Panigrahi, P. K., Pradhan, A., & Ghosh, N. (2014). Fractal anisotropy in tissue refractive index fluctuations: potential role in precancer detection. In J. Popp, V. V. Tuchin, D. L. Matthews, F. S. Pavone, & P. Garside (Eds.), *Proceedings Volume 9121, Biophotonics: Photonic solutions for better health care IV* (91290V). SPIE.
- Falconer, K. (2007). *Fractal geometry: Mathematical foundations and applications*. John Wiley & Sons.
- Farshad, M., & Ahmadi, G. (1974). Effect of boundaries on wave propagation in media with microstructure: II. Surface waves in a half-space. *Bulletin of the Seismological Society of America*, 64, 387–392. doi: 10.1785/BSSA0640020387
- Friston, K. J., Frith, C. D., Dolan, R. J., Price, C. J., Zeki, S., Ashburner, J. T., & Penny, W. D. (2004). Analysis of fMRI time series: Linear time-invariant models, event-related fMRI, and optimal experimental design. In R. S. J. Frackowiak, K. J. Friston, C. D. Frith, R. J. Dolan, C. J. Price, S. Zeki, . . . & W. D. Penny (Eds.), *Human brain function* (2nd ed., pp. 793–822). Elsevier.
- Friston, K. J., Ashburner, J., Kiebel, S., Nichols, T., & Penny, W. (2007). *Statistical parametric mapping: The analysis of functional brain images*. Academic Press.
- Fox, M. D. (2005). The human brain is intrinsically organized into dynamic, anticorrelated functional networks. *Proceedings of the National Academy of Sciences*, 102, 9673–9678. doi: 10.1073/pnas.0504136102
- Fransson, P. (2005). Spontaneous low-frequency BOLD signal fluctuations: An fMRI investigation of the resting-state default mode of brain function hypothesis. *Human Brain Mapping*, 26, 15–29. doi: 10.1002/hbm.20113
- Grant, M. M., Thase, M. E., & Sweeney, J. A. (2001). Cognitive disturbance in outpatient depressed younger adults: Evidence of modest impairment. *Biological Psychiatry*, 50, 35–43. doi: 10.1016/s0006-3223(00)01072-6
- Henson, R., Buechel, C., Josephs, O., & Friston, K. (1999). The slice-timing problem in event-related fMRI [Conference paper]. *5th International Conference on Functional Mapping of the Human Brain (HBM'99) and Educational Brain Mapping Course*, June 22–26, Düsseldorf, Germany.
- Kelly, S. P., Gomez-Ramirez, M., & Foxe, J. J. (2008). Spatial attention modulates initial afferent activity in human primary visual cortex. *Cerebral Cortex*, 18, 2629–2636. doi: 10.1093/cercor/bhn022
- Lai, M., Lombardo, M. V., Chakrabarti, B., Sadek, S. A., Pasco, G., Wheelwright, S. J., . . . & Suckling, J. (2010). A shift to randomness of brain oscillations in people with autism. *Biological Psychiatry*, 68, 1092–1099. doi: 10.1016/j.biopsych.2010.06.027
- Li, B. L., El-Shaarawi, A. H., & Piegorsch, W. W. (2002). Fractal dimensions. In A. H. El-Shaarawi, & W. W. Piegorsch (Eds.), *Encyclopedia of environmetrics* (pp. 161–192). John Wiley & Sons.
- Mandelbrot, B. B., & Wallis, J. R. (1968). Noah, Joseph, and operational hydrology. *Water Resources Research*, 4, 909–918. doi: 10.1029/WR004i005p00909
- MATLAB, 2017. version 9.3.0 (R2017b) [Software]. Natick, Massachusetts: The MathWorks Inc.

- Maxim, V. (2005). Fractional Gaussian noise, functional MRI and Alzheimer's disease. *NeuroImage*, *25*, 141–158. doi: 10.1016/j.neuroimage.2004.10.044
- McCauley, J. L. (1993). *Introduction to multifractals. Chaos, dynamics, and fractals*. Springer Press
- Mitchell A. E. (2016). Phenomenological characteristics of autobiographical memories: responsiveness to an induced negative mood state in those with and without a previous history of depression. *Advances in Cognitive Psychology*, *12*, 105–114. doi: 10.5709/acp-0190-8
- Grassberger, P., & Procaccia, I. (1983). Characterization of strange attractors. *Physical Review Letters*, *50*, 346. doi: 10.1103/PhysRevLett.50.346
- Saha, R. K., Debanath, M. K., & Saikia, E. (2020). Multifractal analysis of ZnO nanoparticles. *Materials Science and Engineering: C*, *106*, 110177. doi: 10.1016/j.msec.2019.110177
- Satterthwaite, T. D., Wolf, D. H., Loughhead, J., Ruparel, K., Elliott, M. A., Hakonarson, H., . . . & Gur, R. E. (2012). Impact of in-scanner head motion on multiple measures of functional connectivity: relevance for studies of neurodevelopment in youth. *NeuroImage*, *60*, 623–632. doi: 10.1016/j.neuroimage.2011.12.063
- Schmitt, F., Schertzer, D., & Lovejoy, S. (1999). Multifractal analysis of foreign exchange data. *Applied Stochastic Models and Data Analysis*, *15*, 29–53. doi: 0.1002/(SICI)1099-0747(199903)15:1<29::AID-ASM357>3.0.CO;2-Z
- Sheline, Y. I., Price, J. L., Yan, Z., & Mintun, M. A. (2010). Resting-state functional MRI in depression unmasks increased connectivity between networks via the dorsal nexus. *Proceedings of the National Academy of Sciences*, *107*, 11020–11025. doi: 10.1073/pnas.1000446107
- Suyal, V., Prasad, A., & Singh, H. (2009). Nonlinear time series analysis of sunspot data. *Solar Physics*, *260*, 441–449. doi: 10.1007/s11207-009-9467-x
- Swan, J. S., MacVicar, R., Christmas, D., Durham, R., Rauchhaus, P., McCullough, J. P., & Matthews, K. (2014). Cognitive behavioural analysis system of psychotherapy (CBASP) for chronic depression: Clinical characteristics and six-month clinical outcomes in an open case series. *Journal of Affective Disorders*, *152–154*, 268–276. doi: 10.1016/j.jad.2013.09.024
- Van Dijk, K. R., Sabuncu, M. R., & Buckner, R. L. (2012). The influence of head motion on intrinsic functional connectivity MRI. *NeuroImage*, *59*, 431–438. doi: 10.1016/j.neuroimage.2011.07.044
- Varley, T. F., Craig, M., Adapa, R., Finoia, P., Williams, G., Allanson, J., . . . & Stamatakis, E. A. (2020). Fractal dimension of cortical functional connectivity networks & severity of disorders of consciousness. *PLoS One*, *15*, e0223812. doi: 10.1371/journal.pone.0223812
- Veer, I. M. (2010). Whole brain resting-state analysis reveals decreased functional connectivity in major depression. *Frontiers in Systems Neuroscience*, *4*. doi: 10.3389/fnsys.2010.00041
- Véhel, J. L., & Legrand, P. (2004). Signal and Image Processing with Fraclab. In M. M. Novak (Ed.), *Thinking in Patterns* (pp. 321–322). doi: 10.1142/9789812702746_0032
- Whitfield-Gabrieli, S., & Nieto-Castanon, A. (2012). CONN: A functional connectivity toolbox for correlated and anticorrelated brain networks. *Brain Connectivity*, *2*, 125–141. doi: 10.1089/brain.2012.0073
- Zeng, L., Shen, H., Liu, L., Wang, L., Li, B., Fang, P., . . . & Hu, D. (2012). Identifying major depression using whole-brain functional connectivity: A multivariate pattern analysis. *Brain*, *135*, 1498–1507. doi: 10.1093/brain/aws059
- Zeng, L. L., Wang, D., Fox, M. D., Sabuncu, M., Hu, D., Ge, M., . . . & Liu, H. (2014). Neurobiological basis of head motion in brain imaging. *Proceedings of the National Academy of Sciences of the United States of America*, *111*, 6058–6062. doi: 10.1073/pnas.1317424111
- Zhou, Y., Yu, C., Zheng, H., Liu, Y., Song, M., Qin, W., . . . & Jiang, T. (2010). Increased neural resources recruitment in the intrinsic organization in major depression. *Journal of Affective Disorders*, *121*, 220–230. doi: 10.1016/j.jad.2009.05.029

RECEIVED 02.09.2021 | ACCEPTED 12.11.2021